Colloid and Polymer Science
https://doi.org/10.1007/s00396-023-05187-x

RESEARCH

A green and sustainable approach to the fabrication of ZnO nanoparticles via *Jatropha podagrica* leaf extract for effective dye degradation and antibacterial applications

Venkatesh Golthi[1,2,3] · Jayarao Kommu[1,3] · A. V. Ramesh[4]

Received: 19 August 2023 / Revised: 13 October 2023 / Accepted: 16 October 2023

Abstract
A robust green synthesis method was employed using *Jatropha podagrica* (Buddha belly plant) leaf extract as a capping agent to prepare ZnO nanoparticles (ZnO NPs). Several analytical techniques such as XRD, SEM, SEM-EDX, HR-TEM, FT-IR, and UV-visible spectroscopy were employed to characterize the green synthesized JP-ZnO NPs. The XRD, SEM, and HR-TEM images proved the presence of spherical nanoparticles having a wurtzite crystalline structure with a size of 12 to 18 nm. The characteristic vibration mode of the Zn-O bond was observed at 430 cm^{-1} in the FT-IR spectrum. The photocatalytic performance of these NPs was evaluated through the degradation of Rhodamine B (RhB), Fluorescein Sodium (FS), and Crystal Violet (CV) dyes in sunlight. Degradation rates of 90–95% were achieved in a time span of 1–2 h. The synthesized ZnO nanoparticles were efficient antimicrobial agents against gram-positive (*Staphylococcus aureus*, *Bacillus coagulans*) and gram-negative (*Klebsiella pneumoniae*, *Escherichia coli*) bacterial strains. Using the well diffusion method, with 150 µL of JP-ZnO nanoparticles, inhibition zones measuring 17, 15, 11, and 10 mm were formed. The current study highlights the efficiency of synthesized JP-ZnO nanoparticles in removing the dyes from aqueous solutions and their efficient antimicrobial properties.

Keywords ZnO nanoparticle · *Jatropha podagrica* plant · Dye degradation · Antioxidant activity

Introduction

In the contemporary world, there has been a continuous increase in industrialization and population growth, leading to the release of various new pollutants into aquatic environments. Specifically, the discharge of noxious dye effluents from industries like textile, paper, leather, and printing poses grave ecological and health hazards [1, 2]. Dyes such as Rhodamine B (RhB), Fluorescein Sodium (FS), and Crystal Violet (CV) pose ingestion risks to humans and animals and induce skin, ocular, and respiratory irritation [3]. In a different context, the recurrence of contagious illnesses and the ongoing evolution of antibiotic resistance in numerous disease-causing bacteria present a significant global public health concern. *Enterococcus*, *Staphylococcus*, and *Streptococcus*, which are closely related species, are harmful microorganisms that are attributed to a diverse range of infections and diseases [4].

In the realm of recent advancements in nanotechnology, nanomaterials play a crucial role due to their significant surface area and volume ratio [5]. This characteristic makes them valuable for applications such as water purification and the creation of novel biocidal substances. Among various types of nanoparticles, zinc oxide nanoparticles (ZnO NPs) possess exceptional optical and electrical characteristics, making them an outstanding choice for *n*-type semiconductor materials [6]. These NPs demonstrate remarkable efficacy in dye degradation [6, 7] and also exhibit antibacterial properties [8, 9], further highlighting their distinctiveness.

✉ Venkatesh Golthi
venkatesh@gdcc.ac.in

1 Andhra University Trans-Disciplinary Research Hub (A.U. TDR-HUB), Visakhapatnam 530003, AP, India

2 Department of Chemistry, Government Degree College, Chodavaram 531036, AP, India

3 Department of Chemistry, Wellfare Institute of Science, Technology and Management, Pinagadi, Pendurthi 531173, AP, India

4 Department of Chemistry, Dr. V.S. Krishna Govt. Degree College, Visakhapatnam 530003, AP, India

Published online: 28 October 2023

Numerous techniques have been documented for the production of ZnO NPs, including hydrothermal [10], precipitation [11], microwave [12], microemulsion [13], solvothermal [14], supercritical water [15], and sol-gel methods [16]. Recent progress in nanotechnology has spurred the rise of sustainable synthesis approaches for generating ZnO NPs [17, 18]. These environmentally synthesized ZnO NPs have garnered substantial interest for their prospective utilization across diverse domains, encompassing dye degradation and antibacterial functionalities. The utilization of these NPs offers a promising solution for addressing environmental challenges associated with dye pollution and combating the spread of drug-resistant bacteria. By harnessing the unique properties of green-synthesized ZnO NPs, researchers aim to explore their efficacy in degrading dyes and inhibiting the growth of pathogenic bacteria, presenting a sustainable and effective approach for environmental and healthcare applications [17–19]. This article delves into the dye degradation and antibacterial activity of ZnO NPs synthesized through green methods, shedding light on their potential as eco-friendly alternatives in addressing pressing global concerns [20–23].

Jatropha podagrica (JP), a traditional medicinal plant, has a history of being utilized for treating various ailments like fever, scabies, ulcers, and wounds. Additionally, it exhibits several beneficial properties including antitumorigenic, antioxidant, and antibacterial activities [24]. The leaves of *Jatropha podagrica* have been analyzed and found to contain specific phytochemicals, namely, flavonoids (such as apigenin, acacetin, and luteolin), phenolic acids (including vanillic, syringic, P-hydroxybenzoic acid, melilotic, cis-trans ferulic, P-coumaric, and phloretic acids), tannins, proanthocyanidins, and glycol flavones [25, 26]. ZnO NPs were successfully produced using leaf extract from the *Jatropha podagrica* plant for the first time. The phytochemicals found within the extract played a crucial and multifaceted role in the *Jatropha podagrica*-capped ZnO nanoparticle (JP-ZnO NP) synthesis, serving both as capping agents and enhancing stability, surpassing that achieved through conventional chemical synthesis methods [25]. Moreover, the presence of diverse phenolic acids within these phytochemicals contributes to achieving well-defined sizes and shapes of ZnO NPs, outperforming analogous green-synthesized counterparts (as depicted in Table 1). To unlock the full potential of unexplored plant species, the selection of new and unique plants for nanoparticle synthesis is imperative. This approach allows researchers to diversify the spectrum of nanoparticles that can be effectively stabilized, achieved through the discovery of novel proteins and phytochemicals derived from previously uninvestigated plant sources. Additionally, these novel plant species may offer additional advantages such as heightened productivity, reduced costs, or specialized attributes suitable for specific applications. In the present research, JP-ZnO nanoparticles displayed a surface with a negative charge, providing them with outstanding adsorption properties for efficiently eliminating Rhodamine B (RhB), Fluorescein Sodium (FS), and Crystal Violet (CV) dyes. Additionally, the antibacterial effectiveness of these manufactured JP-ZnO NPs was evaluated against both Gram-positive bacteria (*Staphylococcus aureus*, *Bacillus coagulans*) and Gram-negative bacteria (*Klebsiella pneumoniae*, *Escherichia coli*).

Table 1 Comparison of the average size and morphology of ZnO nanoparticles in the present work with previous publications

Plant materials	Precursor name	Average size and morphology	Applications	Reference
Jatropha podagrica leaf extract	$Zn(OOCCH_3)_2.2H2O$	12–18 nm and spherical shape	Dye degradation and antibacterial applications	Present work
Calotropis procera extract	$Zn(NO_3)_2.6H2O$	24 nm and spherical shape	Photodegradation of methyl orange	[17]
Solanum torvum L. leaf extract	$Zn(NO_3)_2.6H2O$	28.24 and spherical shape	Toxicological studies	[27]
Simarouba glauca leaf extract	$Zn(NO_3)_2.6H2O$	17–37 nm and hexagonal shape	Antioxidant and antimitotic properties	[28]
Aegle marmelos fruit juice	$Zn(NO_3)_2.6H2O$	17 nm and hexagonal shape	Photodegradation, antibacterial and antioxidant	[29]
Punica granatum leaf extract	$Zn(NO_3)_2.6H2O$	20 nm and spherical shape	Photocatalytic degradation	[30]
Pelargonium zonale leaf extract	$Zn(NO_3)_2.6H2O$	50–60 nm and spherical in shape	Antibacterial activities	[31]
Azadirachta indica leaf extract	$Zn(NO_3)_2.6H2O$	100–200 nm and triangular shape	Antimicrobial activity	[32]
Tetraselmis indica extract	$Zn(OOCCH_3)_2.2H2O$	20–40 nm and spherical shape	Antibacterial, antioxidant, and hemolytic activity	[33]
Aesculus hippocastanum extract	$Zn(OOCCH_3)_2.2H2O$	40 nm and hexagonal shape	Antibacterial activities	[34]
Sechium edule leaf extract	$Zn(OOCCH_3)_2.2H2O$	36.2 nm and spherical shape	Antibacterial and anticancer studies	[35]

Materials and methods

Materials

Fresh *Jatropha podagrica* leaves were picked from the garden of the Government Degree College in Chodavaram, Andhra Pradesh, India. The initial source, zinc acetate dihydrate $Zn(OOCCH_3)_2.2H_2O$ (98% purity), sodium hydroxide (NaOH), Rhodamine B (RhB), Fluorescein Sodium (FS), and Crystal Violet (CV) were acquired from Merck in India and utilized without purification. Milli-Q water was utilized in all of the experiments.

Jatropha podagrica leaf extract preparation

Fresh JP plant leaves were collected and meticulously cleansed using warm water, followed by thorough rinsing with Milli-Q water. These leaves were then dried under shaded conditions for a duration of 25 days until completely dry. Once dry, the leaves were ground into a fine powder using a grinder. Subsequently, 1 g of the powdered sample was placed in a 250-mL glass beaker, and 100 mL of Milli-Q water was added. The blend was subsequently warmed using a heating mantle at 80 °C for 30 min, yielding a brilliant golden-yellow solution. The solution was meticulously sieved using Whatman grade 1 filter paper to eliminate any particulate matter and subsequently subjected to centrifugation at 8000 rpm for 5–10 min to attain a pristine extract solution. The resultant extract was then carefully stored in a refrigerator at 4 °C for subsequent processing [36].

Synthesis of *Jatropha podagrica*-capped ZnO nanoparticles

In a standard eco-friendly synthesis procedure, 10 mL of the aqueous extract derived from JP leaves was blended with 100 mL of a 2 mM aqueous solution containing zinc acetate dihydrate. The amalgamation was subjected to stirring at 80 °C for 30 min, leading to the creation of a vivid yellow solution. Following this, a 1 M solution of sodium hydroxide was meticulously introduced dropwise into the mixture, with uninterrupted agitation at ambient temperature. As a result, the yellow color of the mixture gradually transformed into a yellowish-white suspension, reaching a pH of 12. To purify the suspended particles, they were dispersed in Milli-Q water and then centrifuged at a speed of 8000 rpm. The resultant white particles underwent repeated washing with Milli-Q water to purge impurities and yield the ultimate product. The white solid was then subjected to vacuum drying at 60 °C for 6 h in an oven. Lastly, the material was finely pulverized using a mortar and pestle, rendering it ready for subsequent characterization [36, 37].

Photocatalytic potential of JP-ZnO NPs for the degradation of RhB, FS, and CV dyes

The photocatalytic effectiveness of JP-ZnO NPs against RhB, FS, and CV dyes was assessed using a readily available source of UV radiation — sunlight. In separate containers, 0.01 g of JP-ZnO NPs was blended with 100 mL of 1 ppm solutions of RhB, FS, and CV dyes. To ensure the stability of the solutions against adsorption–desorption phenomena, the reaction mixtures were gently stirred in the absence of light for a duration of 1 h. After stabilization, the solutions were maintained in the sunshine with constant stirring using magnetic stirrers at pH 10. At regular intervals, constant samples were taken from each dye solution and the NPs were separated in a centrifuge at 8000 rpm. A UV spectrometer was used to measure the color intensities at 555 nm, 495 nm, and 590 nm for the RhB, FS, and CV dyes, respectively. The proportion of photocatalytic degradation and rate constants were calculated using the equation below:

$$\text{Degradation rate } (\%) = \left(\left(A_0 - A\right)/A_0\right) \times 100$$

$$\ln A_0/A = kt$$

In the equation, "A_0" symbolizes the initial concentration, while "A" denotes the concentration at the culmination of the degradation process. The degradation constant is denoted by k, and t indicates the duration of sunlight irradiation [38].

Characterization of JP-ZnO NPs

To ascertain the crystalline arrangement of the JP-ZnO NPs, a variety of analytical methodologies were applied. X-ray diffraction (XRD) measurements were carried out across a 2θ range of 0 to 90° using a Bruker Kappa Apex II instrument. The instrument was operated with CuKα radiation ($\lambda = 1.54060$ Å) at settings of 40 kV, 35 mA, and a scanning rate of 0.2 s. Fourier transform infrared spectra (FT-IR) of the samples were captured utilizing a Thermo Nicolet iS50 spectrometer. Spectra were acquired within the frequency span of 4000–400 cm^{-1}, using high-quality KBr pellets in transmission mode. For an in-depth investigation of the optical attributes, UV-Vis diffuse reflectance/absorbance spectroscopy was conducted on the synthesized samples. A Shimadzu (2450 – SHIMADZU) spectrophotometer, equipped with a diffuse reflectance accessory, was deployed under room temperature conditions. $BaSO_4$ was utilized as a reference material, and measurements were executed over the wavelength range of 200–800 nm. The surface topography and elemental composition of the JP-ZnO NPs were

scrutinized through scanning electron microscopy (SEM). The specific apparatus employed was the JEOL 6390LA/OXFORD XMX N, which featured energy-dispersive X-ray (EDX) spectroscopy. SEM images were recorded with an acceleration voltage of 20 kV. For a more comprehensive exploration of the microstructure and particle dimensions, high-resolution transmission electron microscopy (HRTEM) was engaged. The JEOL/JEM 2100 instrument was utilized at an operational voltage of 200 kV. Carbon-copper grids were used for sample preparation, enabling the acquisition of micrographs that facilitated particle size determination. Furthermore, selected area electron diffraction (SAED) images were captured utilizing the HRTEM instrument.

Results and discussions

UV-Vis spectroscopy studies

Figure 1 illustrates the UV-Vis absorption spectra of both JP leaf extract and JP-ZnO NPs. The leaf extract comprises a diverse array of phytochemicals, encompassing alkaloids, phenolic acids, flavonoids, tannins, proanthocyanidins, and glycol flavones. These compounds contribute to pronounced absorption bands at 280 and 351 nm [24]. Additionally, a well-defined absorption peak at 372 nm in the spectra signifies the presence of JP-ZnO NPs, predominantly arising from their capacity to absorb and scatter light [39]. Notably, the absence of absorption peaks at 280 and 351 nm in the JP-ZnO NPs spectra, which were originally observed in the JP leaf extract, implies that these phytochemicals play a pivotal role in the reduction and encapsulation of JP-ZnO NPs during the synthesis process [40].

FTIR analysis of the synthesized JP-ZnO NPs

FTIR spectroscopy was employed to discern the specific functional groups existing within the synthesized NPs and to ascertain their molecular composition. To examine the data concerning functional groups found in the plant (as depicted in Fig. 2), it is evident that a wide peak detected at approximately 3500 cm^{-1} signifies the presence of a phenolic group. Additionally, the identification of aromatic compounds is supported by the absorption of a broad peak around 1639 cm^{-1}. Furthermore, the peaks observed at 1178.39 cm^{-1} and 1042.36 cm^{-1} indicate the existence of amide functional groups and carbonated functional group vibrations within the plant. JP-ZnO NPs were analyzed (as shown in Fig. 2), and their absorption peaks were found to be in the range of 400–4000 cm^{-1}. The peak at 429.08 cm^{-1} indicates the stretching frequency of Zn-O bonding [41]. Peaks observed at 917.20, 901.10, and 795 cm^{-1} can be assigned to carbonate moieties. The occurrence of the symmetric stretching of carboxyl side groups within the amino acid residues of protein molecules is potentially ascribed to

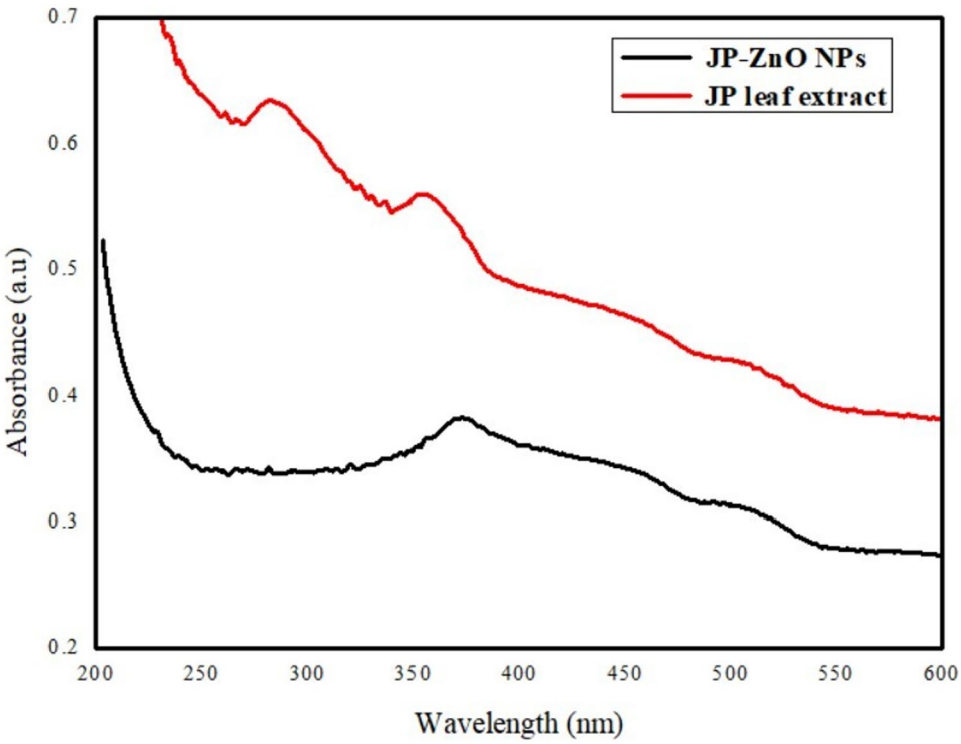

Fig. 1 UV-Vis spectra of *Jatropha podagrica* (JP) leaf extract and *Jatropha podagrica* leaf extract-capped ZnO NPs

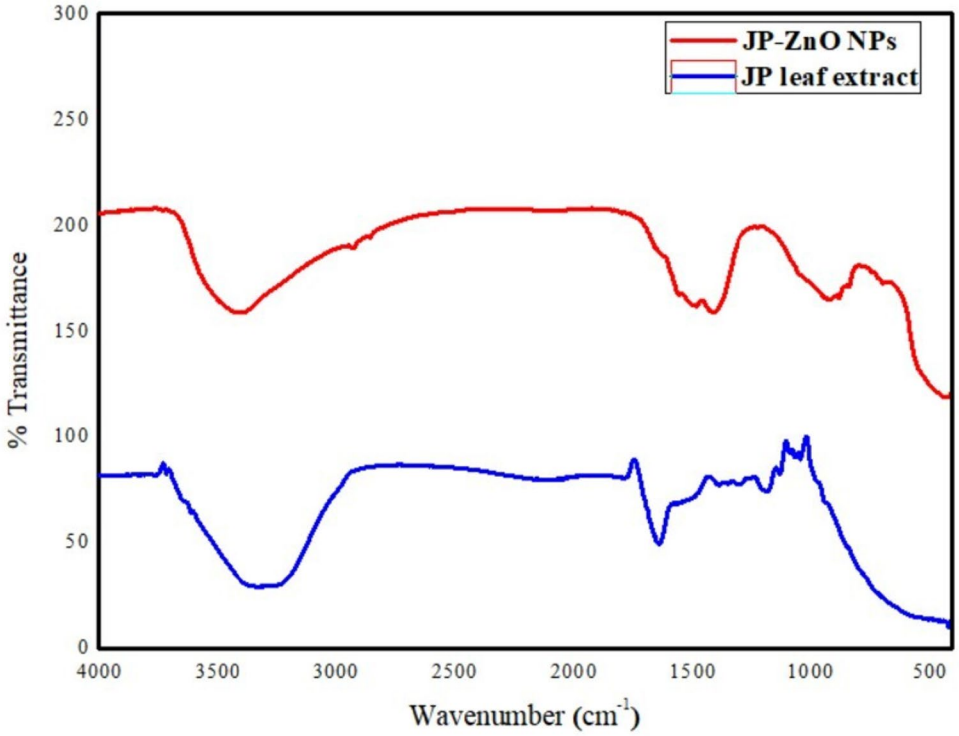

Fig. 2 FTIR spectra of *Jatropha podagrica* leaf extract and *Jatropha podagrica* leaf extract-capped ZnO NPs

the peak at 1410.06 cm^{-1} [42]. The presence of a peak within the 1550- to 1450-cm^{-1} range is likely linked to the C=C stretching of aromatic compounds [43]. Evident and robust absorption bands at 3397.10 and 2923.56 cm^{-1} were identified, signifying the −OH stretching vibration intrinsic to phenolic groups and the −CH stretching vibration characteristic of aldehyde groups [44, 45]. These distinctive peaks within the IR spectrum serve as indicators of the purity and compositional makeup of the biofabricated JP-ZnO NPs.

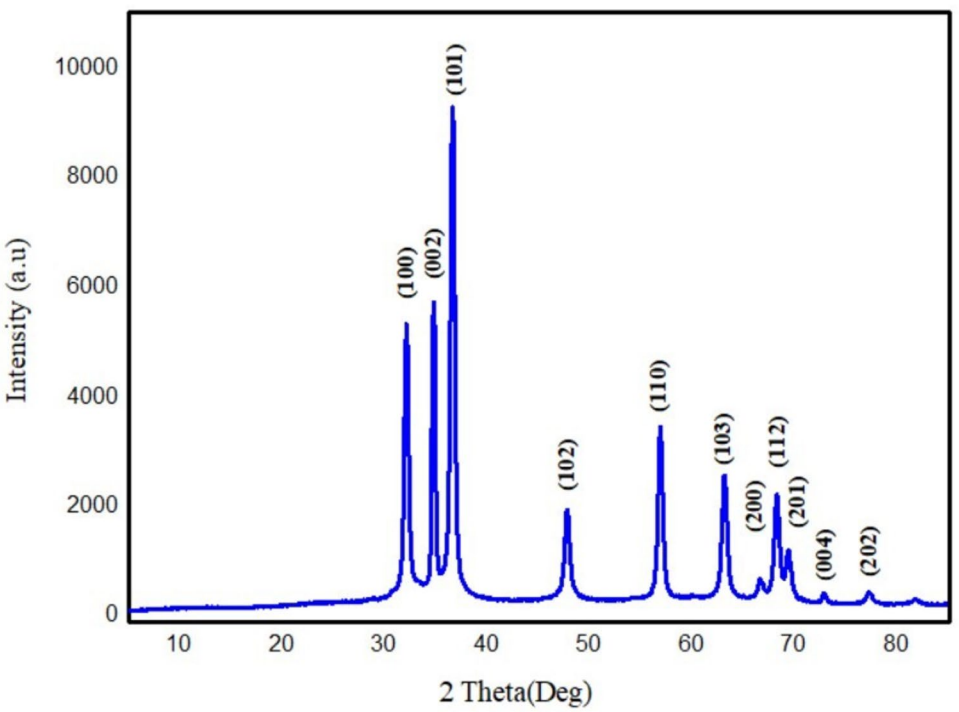

Fig. 3 XRD patterns of ZnO NPs using an aqueous leaf extract of *Jatropha podagrica*

Table 2 The structure and geometric parameters of JP-ZnO NPs

Planes	2θ	β	cosθ	Size (nm)
100	31.98	0.53635	0.96131	14.23869
002	34.63	0.41516	0.954683	18.26832
101	36.47	0.52835	0.949781	14.28094
102	47.75	0.71887	0.914431	10.10545
110	56.82	0.59138	0.879566	11.81562
103	63.07	0.67663	0.852321	10.00707
200	66.68	1.30914	0.835424	5.069625
112	68.17	0.6336	0.828207	10.38434
201	69.28	0.74629	0.82274	8.7581
004	72.76	0.37226	0.805101	17.18142
202	77.18	0.40693	0.781629	15.25936
Average size				**12.30627**

XRD analysis of the synthesized JP-ZnO NPs

The X-ray diffraction analysis, as shown in Fig. 3, revealed distinctive peak characteristic of JP-ZnO at various angles: 31.98°, 34.63°, 36.47°, 47.75°, 56.82°, 63.07°, 66.68°, 68.17°, 69.28°, 72.76°, and 77.18°. These peaks corresponded to different crystal lattice planes, including (100), (002), (101), (102), (110), (103), (200), (112), (201), (004), and (202), respectively. The congruence of these peaks with the established JCPDS Card No. 89–0510 indicated the presence of ZnO NPs in the wurtzite crystalline structure. The well-defined and narrow diffraction peaks attested to a robust crystalline structure, while the absence of other signals verified the purity of the synthesized JP-ZnO NPs. Notably, the intensity of the (002) peak indicated the

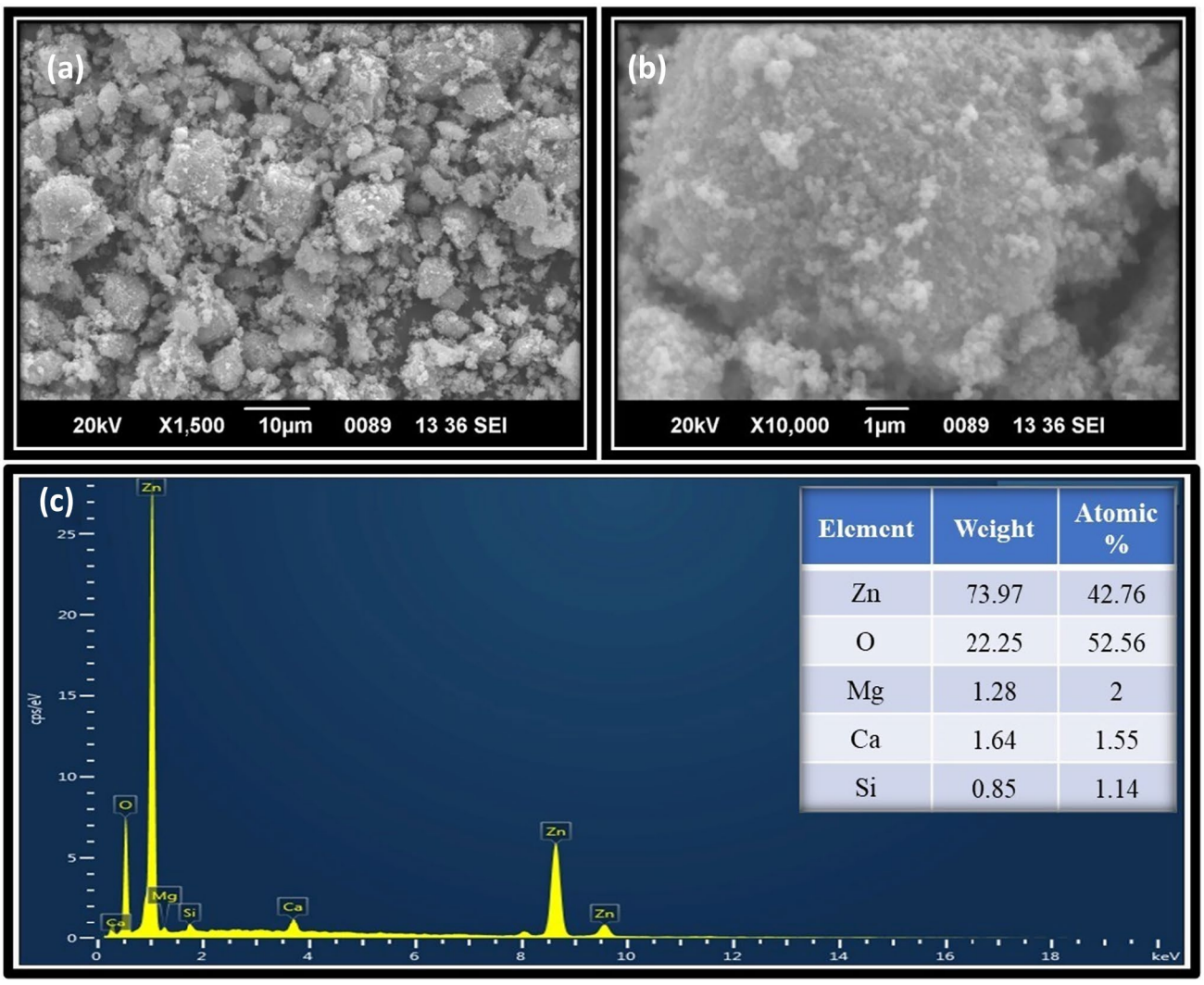

Fig. 4 **a** and **b** SEM images ZnO NPs capped with *Jatropha podagrica* leaf extract different magnifications and **c** EDX spectrum of ZnO NPs

spherical morphology of the particles [46]. To calculate the average grain size of the samples, the Debye-Scherer equation was employed: $D = k\lambda/\beta\cos\theta$. Here, D represents the crystal size, λ stands for the wavelength of X-ray radiation ($\lambda = 0.15406$ nm) for Cu Kα, k is the shape factor (typically taken as 0.9), β denotes the full width at half maximum (FWHM), and θ represents the diffraction angle.

Table 2 represents the structure and geometric parameters of JP-ZnO NPs.

Employing the Debye-Scherer equation, the average size of the crystallites within the JP-ZnO NPs was computed to be 12.30627 nm (Table 2), confirming their nanoscale dimensions.

SEM-EDX analysis of synthesized JP-ZnO NPs

The surface characteristics of the produced JP-ZnO NPs were examined using a scanning electron microscope (SEM). As depicted in Fig. 4(a), (b), the particles exhibited predominantly wurtzite crystalline structure and a spherical shape [47]. Some clustering of particles was observed, likely attributed to the presence of phenolic

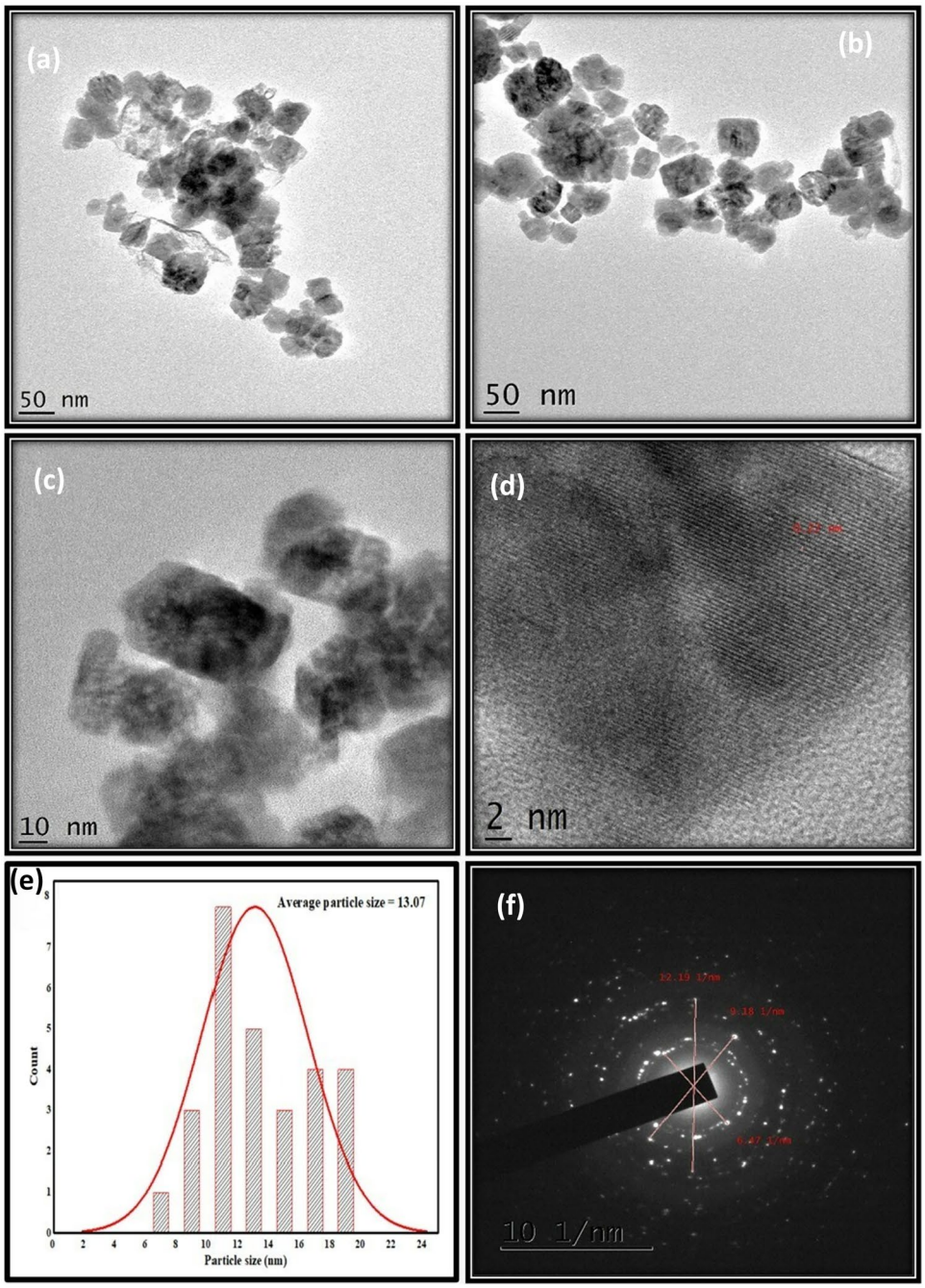

Fig. 5 **a**–**d** HR-TEM images, **e** size distribution histogram of using aqueous *Jatropha podagrica* leaf extract of ZnO NPs, and **f** SAED patterns

compounds from the JP plant, which acted as a capping agent. To determine the chemical constitution of the ZnO NPs, an energy-dispersive X-ray spectrum (EDX) was obtained from a densely populated region (Fig. 4(c)). The EDX spectrum revealed significant signals from zinc atoms at 1 keV, 8.7 keV, and 9.6 keV, respectively, along with a single peak corresponding to oxygen atoms at 0.5 keV. The presence of a negligible amount of carbon atoms confirmed the high purity of the NPs. Additionally, minor peaks representing calcium (Ca), magnesium (Mg), and silicon (Si) atoms were detected, indicating the contribution of these elements from the biological components.

TEM analysis of synthesized JP-ZnO NPs

The dimensions, arrangement, and architecture of the synthesized JP-ZnO NPs underwent meticulous scrutiny through high-resolution transmission electron microscopy (HR-TEM). HR-TEM images at varying magnifications are showcased in Fig. 5(a–c). Scrutinizing these images unveiled that the average size of the JP-ZnO NPs resides within the range of 12–18 nm. Impressively, a measured "*d*" spacing of 0.22 nm harmonized with the *d* values derived from X-ray diffraction (XRD), thereby affirming the ZnO NPs' wurtzite crystalline structure and spherical morphology [48], as visualized in Fig. 5(d). Significantly, Fig. 5(e) underscores that the particle size deduced from the HR-TEM analysis exhibited commendable concurrence with outcomes from the XRD analysis. The selected area electron diffraction pattern (SAED) of the JP-ZnO NPs is portrayed in Fig. 5(f). The SAED pattern indicated the presence of polycrystalline NPs in the JP-ZnO sample.

Plausible mechanism for fabrication of JP-ZnO NPs

Figure 6 provides an illustrative representation of a potential procedure aimed at producing ZnO NPs utilizing a water-based solution derived from the leaves of

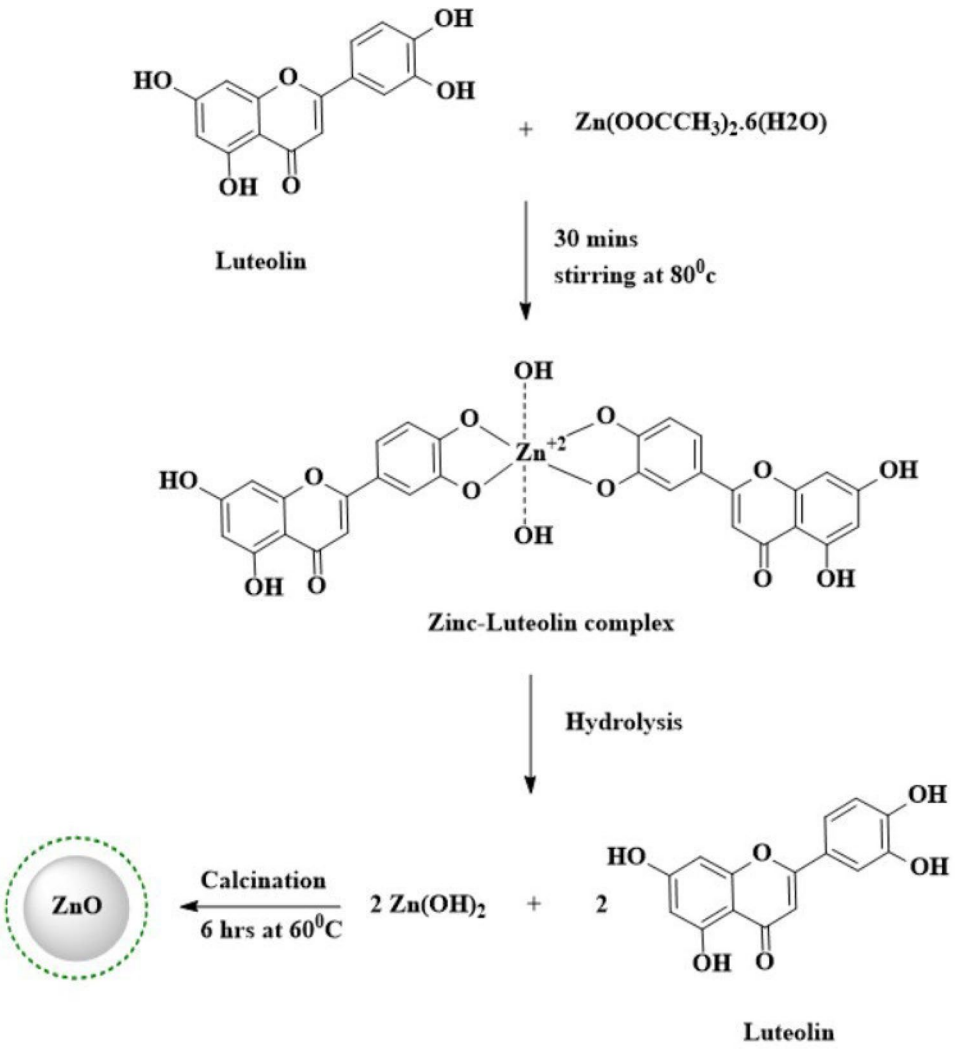

Fig. 6 A proposed mechanism of synthesized ZnO NPs using a *Jatropha podagrica* leaf extract

JP. The procedure involves combining an aqueous leaf extract obtained from JP with zinc acetate hexahydrate ($Zn(OOCCH_3)_2.6H_2O$) within a single aqueous phase. The leaf extract from JP contains a range of constituents, including phenolic acids, flavonoids, tannins, terpenoids, and carbohydrates. These components serve a dual purpose as both reducing and capping agents in the reaction. Notably, a remarkable chemical within the leaf extract is luteolin, which complexes with zinc in the form of Zn^{+2} ions.

This initial complexation is followed by the sequential progression of events. First, there is the conception of zinc hydroxide ($Zn(OH)_2$) via hydrolysis. Subsequently, through a process of calcination, the complex undergoes decomposition [49]. This decomposition process strongly favors the generation of JP-ZnO NPs.

A photocatalytic degradation of RhB, FS, and CV dyes by the fabricated JP-ZnO NPs

To evaluate the photocatalytic activity of prepared JP-ZnO NPs, they were employed as catalysts in the photodegradation of RhB, CV, and FS dyes in sunlight. Figures 7, 8, and 9 demonstrate the degradation of the dyes RhB, FS, and CV under sunlight, occurring at time intervals of 180 min, 90 min, and 60 min, respectively. The UV-visible spectrometer was used to measure the RhB, FS, and CV dye degradation at regular intervals of 30 min, 20 min, and 15 min, respectively. Degradation efficiencies of 95%, 94%, and 90% were achieved for RhB, FS, and CV dyes, respectively. The degradation efficiency of the as-prepared JP-ZnO NPs was compared with that of recently reported ZnO NPs in Table 3.

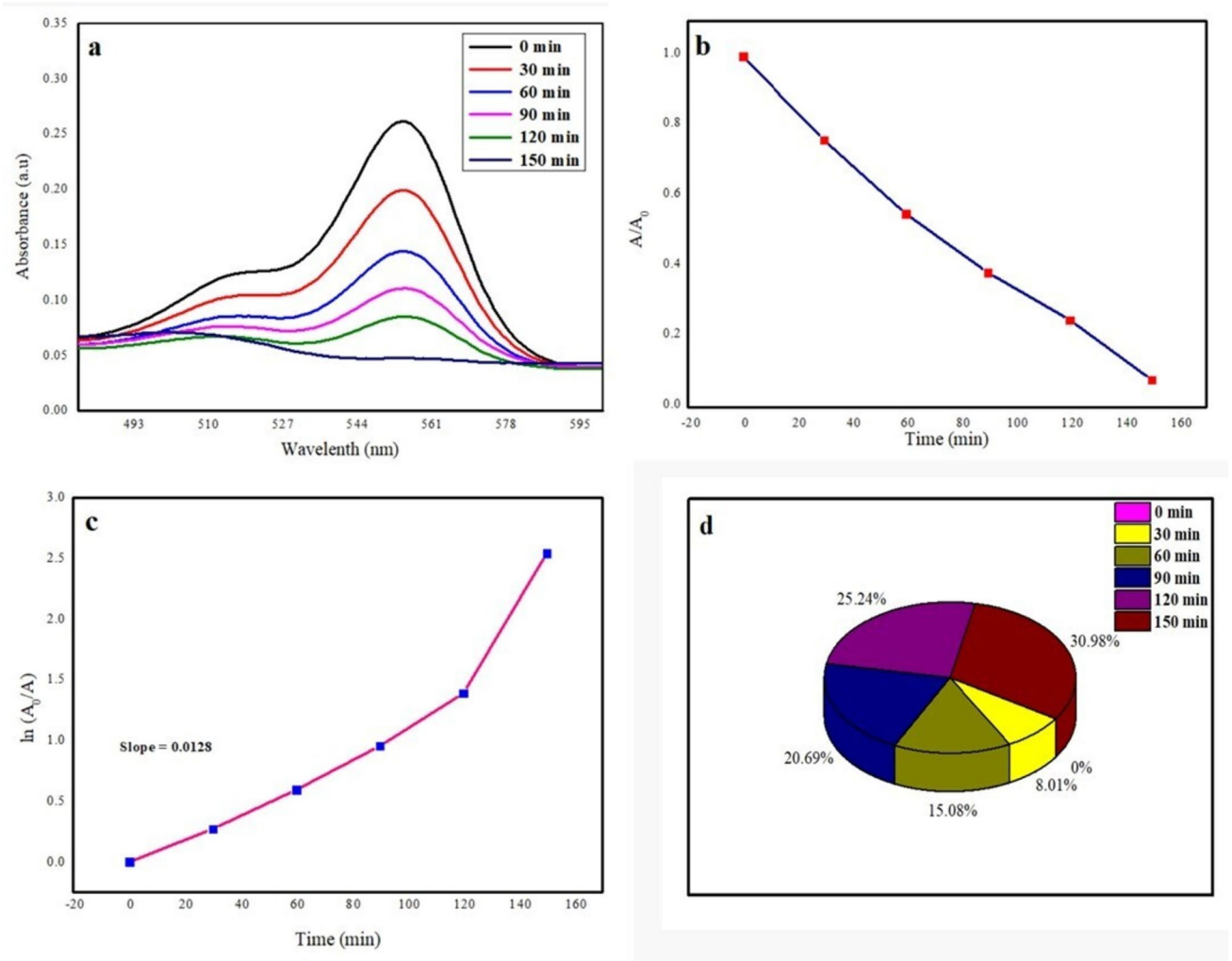

Fig. 7 **a** UV-Vis absorbance spectra of RhB dye under UV (sunlight) illumination over JP-ZnO NPs as a function of time, **b** the progression of RhB dye degradation during consecutive time intervals, **c** the kinetics of RhB dye degradation presented as a first-order linear plot with ln A_0/A as a function of time, and **d** a pie chart representing the distribution of RhB dye degradation across different time intervals

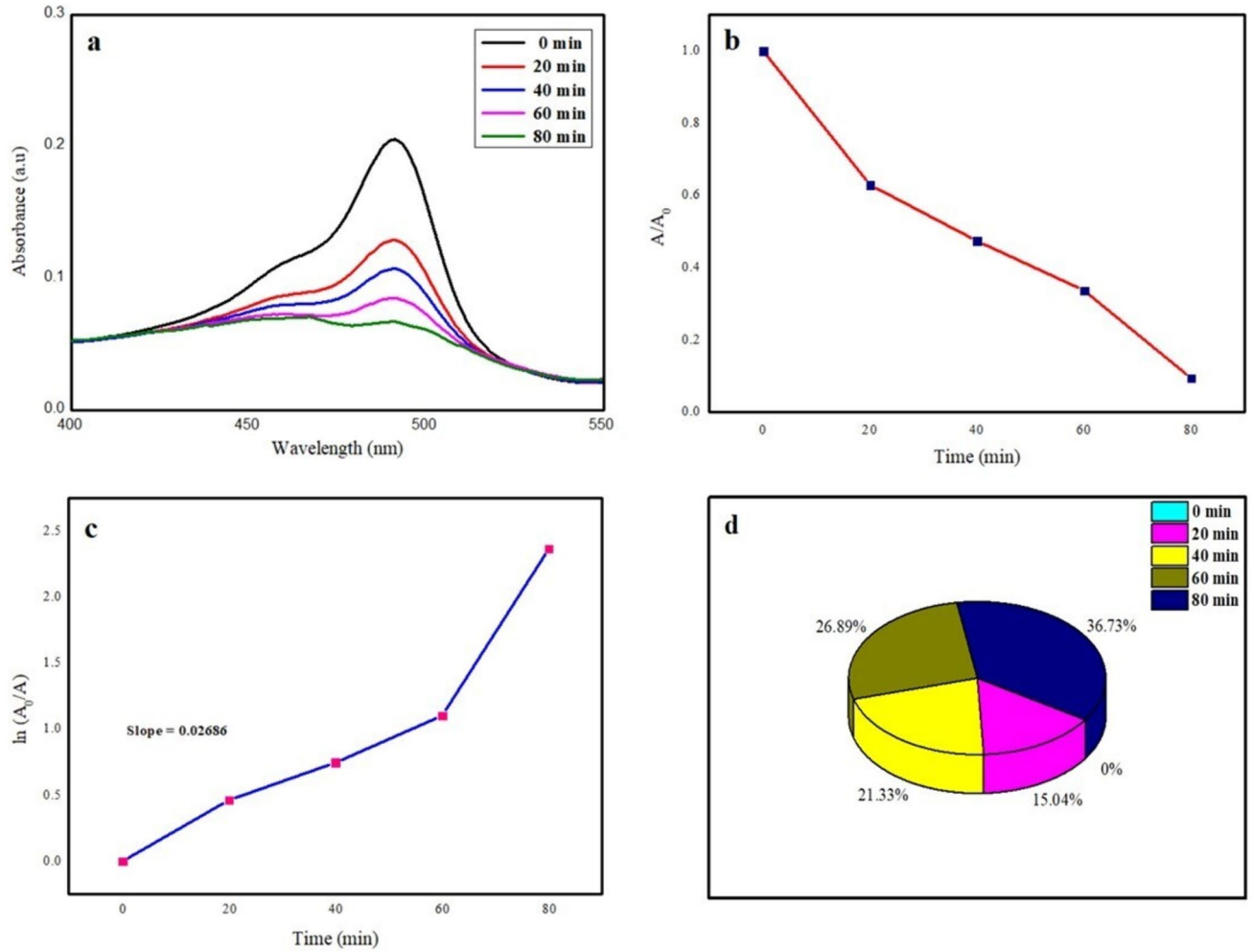

Fig. 8 **a** UV-Vis absorbance spectra of FS dye under UV (sunlight) illumination over JP-ZnO NPs as a function of time, **b** the progression of FS dye degradation during consecutive time intervals, **c** the kinetics of FS dye degradation presented as a first-order linear plot with ln A_0/A as a function of time, and **d** a pie chart representing the distribution of FS dye degradation across different time intervals

The results of this study strongly suggest that JP-ZnO NPs possess significant promise as a material for effectively catalyzing the degradation of organic pollutants through photocatalysis. The remarkable rates of degradation observed, coupled with the observable impact of varying pH conditions on the degradation process, highlight the potential application of JP-ZnO NPs in addressing a wide spectrum of water and wastewater pollution challenges stemming from organic contaminants. These results suggest that JP-ZnO NPs offer promising prospects for addressing environmental pollution challenges.

The following mechanism illustrates how electrons and holes contribute to dye degradation [56]:

$$ZnO + h\nu \rightarrow e^- + h^+$$

O_2 absorption: $O_2 + e^- \rightarrow O_2^-$

Ionization of water: $H_2O \rightarrow OH^- + H^+$

Protonation of superoxide: $O_2^- + H^+ \rightarrow HOO$

$$HOO + e^- \rightarrow HO_2^-$$

$$HOO^- + H^+ \rightarrow H_2O_2$$

$$H_2O_2 + e^- \rightarrow OH^- + OH$$

$$H_2O + h^+ \rightarrow H^+ + OH$$

Dyes + OH. → Degradant product

The aforementioned OH radical is an extremely potent oxidant, highly effective in the degradation of numerous dyes such as RhB, FS, and CV.

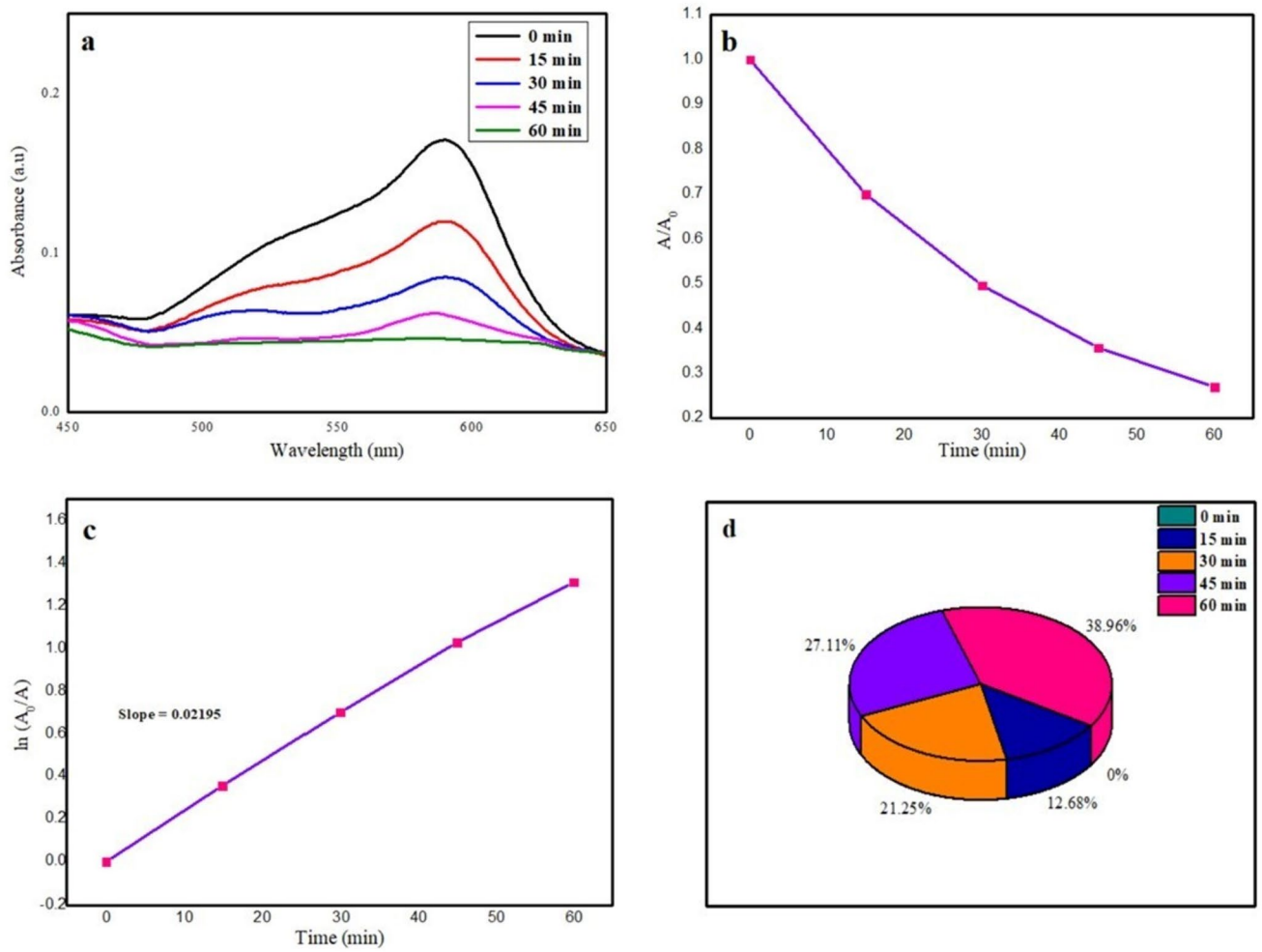

Fig. 9 **a** UV-Vis absorbance spectra of CV dye under UV (sunlight) illumination over JP-ZnO NPs as a function of time, **b** the progression of CV dye degradation during consecutive time intervals, **c** the kinetics of CV dye degradation presented as a first-order linear plot with ln A_0/A as a function of time, and **d** a pie chart representing the distribution of CV dye degradation across different time intervals

Antibacterial activities of synthesized JP-ZnO NPs

The antibacterial effectiveness of JP-ZnO NPs was assessed against both Gram-positive bacteria (*S. aureus*, *B. coagulans*) and Gram-negative bacteria (*K. pneumoniae*, *E. coli*) through the utilization of the well diffusion method. The outcomes of the zone inhibition technique are depicted in Fig. 10, illustrating the diameters of inhibition zones (measured in millimeters) encompassing each well containing the JP-ZnO NP solution. The JP-ZnO NPs prepared for this

Table 3 Comparison of the photocatalytic degradation of ZnO nanoparticles in the present work with previous works

Green materials	Dye	Light source	Irradiation time (min)	Degradation efficiency (%)	Reference
Jatropha podagrica leaf extract	Rhodamine B	Sunlight	150	95	Present work
	Crystal Violet	Sunlight	60	94	
	Fluorescein Sodium	Sunlight	90	90	
Alchemilla vulgaris leaf extract	Rhodamine B	Sunlight	120	75	[50]
Hibiscus sabdariffa L. petal extract	Rhodamine B	Sunlight	300	80.13	[51]
Paraserianthes lophantha leaf extract	Rhodamine B	UV light	180	83	[52]
Moringa oleifera peel extract	Crystal Violet	UV light	70	94	[53]
Delonix elata leaf extract	Crystal Violet	UV light	90	86	[54]
Sageretia thea aqueous extract	Crystal Violet	UV light	8 h	40.65	[55]

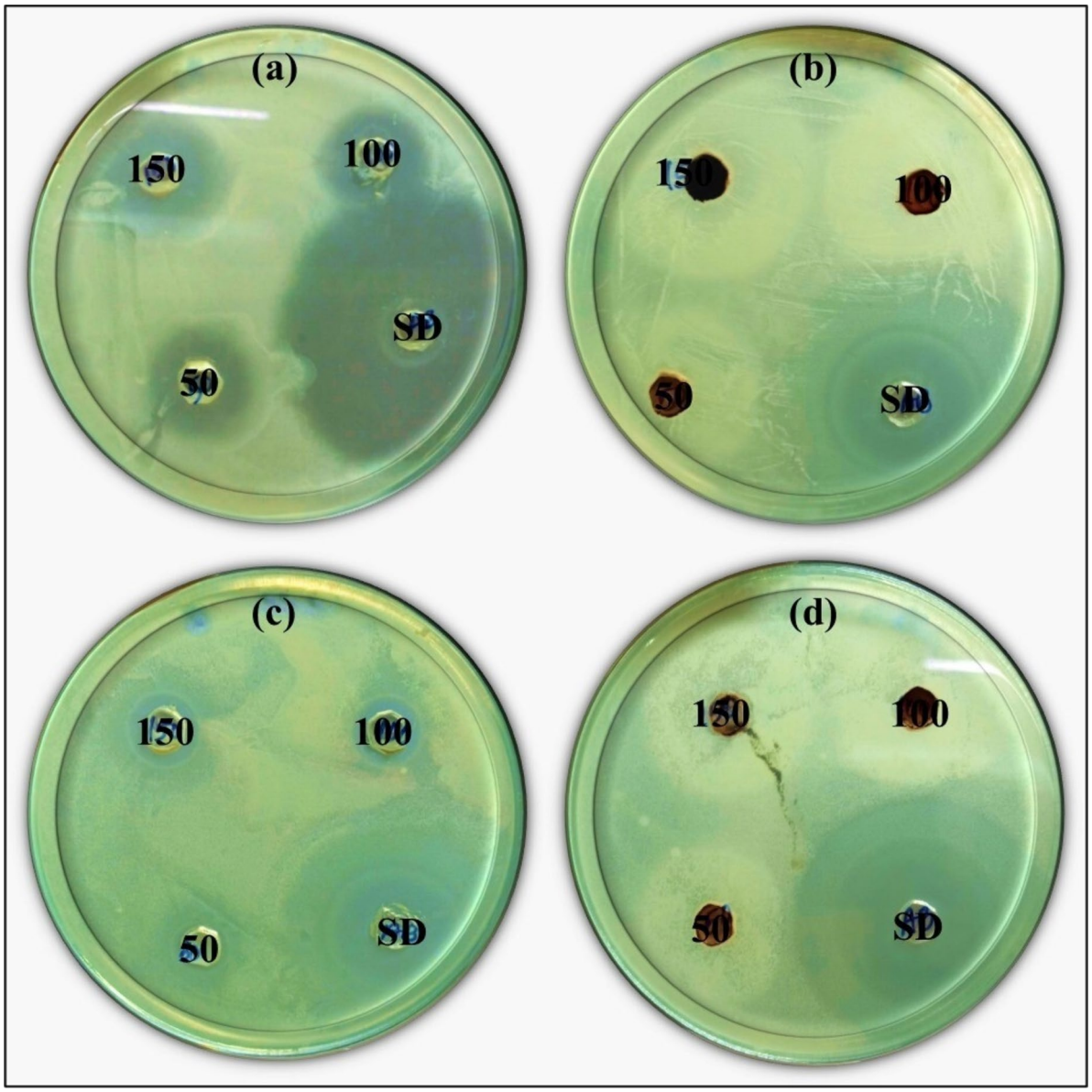

Fig. 10 Antibacterial efficacy of ZnO NPs synthesized using *Jatropha podagrica* leaf extract for **a** *S. aureus*, **b** *B. coagulans*, **c** *K. pneumoniae*, and **d** *E. coli*

study exhibited substantial antibacterial potency against *S. aureus*, *B. coagulans*, *K. pneumoniae*, and *E. coli*. Particularly favorable outcomes were witnessed against *S. aureus* (17 mm), *B. coagulans* (15 mm), *K. pneumoniae* (11 mm), and *E. coli* (10 mm) at a concentration of 150 µL, surpassing the performance of conventional drugs. The plant extract

Table 4 Zone of inhibition at different concentrations of JP-ZnO NPs

Name	*S. aureus*	*B. coagulans*	*K. pneumoniae*	*E. coli*
Shape	Round	Round	Round	Round
Gram reaction	Gram positive	Gram positive	Gram negative	Gram negative
50 µL	15 mm	12 mm	10 mm	10 mm
100 µL	16 mm	13 mm	11 mm	10 mm
150 µL	17 mm	15 mm	13 mm	11 mm
Antibiotic	40 mm	27 mm	40 mm	32 mm

exhibited commendable activity against both Gram-positive and Gram-negative bacteria, resulting in an inhibition zone of 6 mm. At various JP-ZnO NP concentrations, Table 4 shows the zone of inhibition.

From the aforementioned results, the susceptibility of Gram-positive bacteria (*S. aureus*, *B. coagulans*) exhibited a heightened degree of susceptibility to JP-ZnO NPs in contrast to Gram-negative bacteria (*K. pneumoniae*, *E. coli*). This discrepancy in sensitivity can be attributed to the substantial presence of a thick peptidoglycan layer within the cell wall of Gram-positive bacteria, which serves as a robust physical barrier offering shielding and protection. In contrast, Gram-negative bacteria possess both lipopolysaccharide and peptidoglycan, rendering them more resistant to the effects of JP-ZnO NPs [57–59].

Conclusions

In summary, we have successfully employed an eco-friendly method for synthesizing ZnO nanoparticles, using *Jatropha podagrica* leaf extract as a capping agent. Distinct analytical techniques were employed to characterize the nanoparticles which confirmed their wurtzite crystalline structure, spherical shape, and size in the range of 12 to 18 nm. The JP-ZnO nanoparticles have demonstrated a remarkable photocatalytic efficiency, effectively breaking down RhB, FS, and CV dyes under sunlight. The degradation rates of 90–95% were achieved within a time frame of 150, 90, and 60 min for RhB, FS, and CV dyes. We evaluated their antibacterial properties against both gram-positive (*S. aureus*, *B. coagulans*) and gram-negative (*K. pneumoniae*, *E. coli*) bacterial strains. Using 150 µL of nanoparticles, inhibition zones measuring 17, 15, 11, and 10 mm were obtained. These findings highlight the potential applications of JP-ZnO nanoparticles in addressing water pollution challenges and formulating potent antibacterial agents.

Acknowledgements The authors express sincere gratitude to Dr. K. Basavaiah, professor in the Department of Analytical Chemistry at Andhra University, Visakhapatnam, Andhra Pradesh, India, for generously facilitating UV-Vis spectroscopy for the purpose of characterizations.

Author contribution Venkatesh wrote the manuscript and prepared the tables and figures, A. V. Ramesh collected the data, and Jayarao reviewed the manuscript.

Availability of data and materials This declaration is "not applicable" .

Declarations

Ethical approval This declaration is "not applicable".

Competing interests The authors declare no competing interests.

References

1. Lee KM, Lai CW, Ngai KS, Juan JC (2016) Recent developments of zinc oxide based photocatalyst in water treatment technology: a review. Water Res 88:428–448. https://doi.org/10.1016/j.watres.2015.09.045
2. Weber R, Watson A, Forter M, Oliaei F (2011) Review Article: Persistent organic pollutants and landfills — a review of past experiences and future challenges. Waste Manag Res 29(1):107–121. https://doi.org/10.1177/0734242X10390730
3. Jain R, Mathur M, Sikarwar S, Mittal A (2007) Removal of the hazardous dye rhodamine B through photocatalytic and adsorption treatments. J Environ Manage 85(4):956–964. https://doi.org/10.1016/j.jenvman.2006.11.002
4. Jones N, Ray B, Ranjit KT, Manna AC (2008) Antibacterial activity of ZnO nanoparticle suspensions on a broad spectrum of microorganisms. FEMS Microbiol Lett 279(1):71–76. https://doi.org/10.1111/j.1574-6968.2007.01012.x
5. Emami-Karvani Z, Chehrazi P (2011) Antibacterial activity of ZnO nanoparticle on gram-positive and gram-negative bacteria. Afr J Microbiol Res 5(12):1368–1373. https://doi.org/10.5897/AJMR10.159
6. Golmohammadi M, Honarmand M, Ghanbari S (2020) A green approach to synthesis of ZnO nanoparticles using jujube fruit extract and their application in photocatalytic degradation of organic dyes. Spectrochim Acta Part A Mol Biomol Spectrosc 229:117961. https://doi.org/10.1016/j.saa.2019.117961
7. Davar F, Majedi A, Mirzaei A (2015) Green synthesis of ZnO nanoparticles and its application in the degradation of some dyes. J Am Ceram Soc 98:1739–1746. https://doi.org/10.1111/jace.13467
8. Raghupathi KR, Koodali RT, Manna AC (2011) Size-dependent bacterial growth inhibition and mechanism of antibacterial activity of zinc oxide nanoparticles. Langmuir 27(7):4020–4028. https://doi.org/10.1021/la104825u
9. Sirelkhatim A, Mahmud S, Seeni A et al (2015) Review on zinc oxide nanoparticles: antibacterial activity and toxicity mechanism. Nano-Micro Lett 7:219–242. https://doi.org/10.1007/s40820-015-0040-x
10. Maryanti E, Damayanti D, Gustian I (2014) Synthesis of ZnO nanoparticles by hydrothermal method in aqueous rinds extracts of *Sapindus rarak* DC. Mater Lett 118:96–98. https://doi.org/10.1016/j.matlet.2013.12.044
11. Ghorbani HR, Mehr FP, Pazoki H, Rahmani BM (2015) Synthesis of ZnO nanoparticles by precipitation method. Orient J Chem 31(2). https://doi.org/10.13005/ojc/310281
12. Ahammed KR, Ashaduzzaman M, Paul SC et al (2020) Microwave assisted synthesis of zinc oxide (ZnO) nanoparticles in a noble approach: utilization for antibacterial and photo catalytic activity. SN Appl Sci 2:955. https://doi.org/10.1007/s42452-020-2762-8
13. Yıldırım ÖA, Durucan C (2010) Synthesis of zinc oxide nanoparticles elaborated by microemulsion method. J Alloy Compd 506(2):944–949. https://doi.org/10.1016/j.jallcom.2010.07.125
14. Ghoshal T, Biswas S, Paul M, De SK (2009) Synthesis of ZnO nanoparticles by solvothermal method and their ammonia sensing properties. J Nanosci Nanotechnol 9(10):5973–5980. https://doi.org/10.1166/jnn.2009.1290
15. Leybros A, Piolet R, Ariane M, Muhr H, Bernard F, Demoisson F (2012) CFD simulation of ZnO nanoparticle precipitation in a supercritical water synthesis reactor. J Supercrit Fluids 70:17–26. https://doi.org/10.1016/j.supflu.2012.06.001
16. Hasnidawani JN, Azlina HN, Norita H, Bonnia NN, Ratim S, Ali ES (2016) Synthesis of ZnO nanostructures using sol-gel method. Procedia Chem 19:211–216. https://doi.org/10.1016/j.proche.2016.03.095
17. Gawade VV, Gavade NL, Shinde HM, Babar SB, Kadam AN, Garadkar KM (2017) Green synthesis of ZnO nanoparticles by

using *Calotropis procera* leaves for the photodegradation of methyl orange. J Mater Sci: Mater Electron 28:14033–14039. https://doi.org/10.1007/s10854-017-7254-2
18. Rathnasamy R, Thangasamy P, Thangamuthu R et al (2017) Green synthesis of ZnO nanoparticles using *Carica papaya* leaf extracts for photocatalytic and photovoltaic applications. J Mater Sci: Mater Electron 28:10374–10381. https://doi.org/10.1007/s10854-017-6807-8
19. Batra V, Kaur I, Pathania D, Chaudhary V (2022) Efficient dye degradation strategies using green synthesized ZnO-based nanoplatforms: a review. Appl Surf Sci Adv 11:100314. https://doi.org/10.1016/j.apsadv.2022.100314
20. Thi TUD, Nguyen TT, Thi YD, Thi KHT, Phan BT, Pham KN (2020) Green synthesis of ZnO nanoparticles using orange fruit peel extract for antibacterial activities. RSC Adv 10(40):23899–23907. https://doi.org/10.1039/D0RA04926C
21. Raj A, Lawrence RS, Jalees MOHAMMAD, Lawrence KAPIL (2015) Anti-bacterial activity of zinc oxide nanoparticles prepared from *Brassica oleraceae* leaves extract. Int J Adv Res 3(11):322–328
22. Ramesh M, Anbuvannan M, Viruthagiri GJSAPAM (2015) Green synthesis of ZnO nanoparticles using *Solanum nigrum* leaf extract and their antibacterial activity. Spectrochim Acta Part A Mol Biomol Spectrosc 136:864–870. https://doi.org/10.1016/j.saa.2014.09.105
23. Espenti CS, Rama Krishna AG, Rami Reddy YV (2020) Green biosynthesis of ZnO nanomaterials and their anti-bacterial activity by using *Moringa Oleifera* root aqueous extract. SN Appl Sci 2:1424. https://doi.org/10.1007/s42452-020-2945-3
24. Bhaskarwar BHUSHAN, Itankar PRAKASH, Fulke ABHAY (2008) Evaluation of antimicrobial activity of medicinal plant *Jatropha podagrica* (Hook). Rom Biotechnol Lett 13(5):3873–3877
25. Thomas S (2016) Pharmacognostic and phytochemical constituents of leaves of *Jatropha multifida* Linn. and *Jatropha podagrica* Hook. J Pharmacogn Phytochem 5(2):243–246
26. Panzu NN, Lengbiye EM, Domondo A, Inkoto CL, Muanyishay CL, Gbolo BZ, Mpiana PT (2020) A review on the bioactivity and phytochemistry of *Jatropha podagrica* Hook (Euphorbiaceae). Discov Phytomedicine 7(4):186–194. https://doi.org/10.15562/phytomedicine.2020.150
27. Ezealisiji KM, Siwe-Noundou X, Maduelosi B et al (2019) Green synthesis of zinc oxide nanoparticles using *Solanum torvum* (L) leaf extract and evaluation of the toxicological profile of the ZnO nanoparticles–hydrogel composite in Wistar albino rats. Int Nano Lett 9:99–107. https://doi.org/10.1007/s40089-018-0263-1
28. Hemanth Kumar, N.K., Murali, M., Satish, A et al (2020) Bioactive and biocompatible nature of green synthesized zinc oxide nanoparticles from *Simarouba glauca* DC: An Endemic Plant to Western Ghats, India. J Clust Sci 31:523–534. https://doi.org/10.1007/s10876-019-01669-7
29. Mallikarjunaswamy C, Lakshmi Ranganatha V, Ramu R et al (2020) Facile microwave-assisted green synthesis of ZnO nanoparticles: application to photodegradation, antibacterial and antioxidant. J Mater Sci Mater Electron 31:1004–1021. https://doi.org/10.1007/s10854-019-02612-2
30. Singh K, Singh J, Rawat M (2019) Green synthesis of zinc oxide nanoparticles using *Punica granatum* leaf extract and its application towards photocatalytic degradation of Coomassie brilliant blue R-250 dye. SN Appl Sci 1:624. https://doi.org/10.1007/s42452-019-0610-5
31. Vahidi A, Vaghari H, Najian Y, Najian M, Jafarizadeh-Malmiri H (2019) Evaluation of three different green fabrication methods for the synthesis of crystalline ZnO nanoparticles using *Pelargonium zonale* leaf extract. Green Process Synth 8(1):302–308. https://doi.org/10.1515/gps-2018-0097
32. Sharma BK, Mehta BR, Shah EV et al (2022) Green synthesis of triangular ZnO nanoparticles using *Azadirachta indica* leaf extract and its shape dependency for significant antimicrobial activity: joint experimental and theoretical investigation. J Clust Sci 33:2517–2530. https://doi.org/10.1007/s10876-021-02145-x
33. Thirumoorthy GS, Balasubramaniam O, Kumaresan P et al (2021) *Tetraselmis indica* mediated green synthesis of zinc oxide (ZnO) nanoparticles and evaluating its antibacterial, antioxidant, and hemolytic activity. BioNanoSci 11:172–181. https://doi.org/10.1007/s12668-020-00817-y
34. Çolak H, Karaköse E, Duman F (2017) High optoelectronic and antimicrobial performances of green synthesized ZnO nanoparticles using *Aesculus hippocastanum*. Environ Chem Lett 15:547–552. https://doi.org/10.1007/s10311-017-0629-z
35. Elavarasan N, Kokila K, Inbasekar G et al (2017) Evaluation of photocatalytic activity, antibacterial and cytotoxic effects of green synthesized ZnO nanoparticles by *Sechium edule* leaf extract. Res Chem Intermed 43:3361–3376. https://doi.org/10.1007/s11164-016-2830-2
36. Varadavenkatesan T, Lyubchik E, Pai S, Pugazhendhi A, Vinayagam R, Selvaraj R (2019) Photocatalytic degradation of Rhodamine B by zinc oxide nanoparticles synthesized using the leaf extract of *Cyanometra ramiflora*. J Photochem Photobiol B 199:111621. https://doi.org/10.1016/j.jphotobiol.2019.111621
37. Darvishi D, Kahrizi D, Arkan E (2019) Comparison of different properties of zinc oxide nanoparticles synthesized by the green (using *Juglans regia* L. leaf extract) and chemical methods. J Mol Liq. https://doi.org/10.1016/j.molliq.2019.04.108
38. Hassan SS, El Azab WI, Ali HR, Mansour MS (2015) Green synthesis and characterization of ZnO nanoparticles for photocatalytic degradation of anthracene. Adv Nat Sci: Nanosci Nanotechnol 6(4):045012. https://doi.org/10.1088/2043-6262/6/4/045012
39. Jayappa MD, Ramaiah CK, Kumar MAP et al (2020) Green synthesis of zinc oxide nanoparticles from the leaf, stem and in vitro grown callus of *Mussaenda frondosa* L.: characterization and their applications. Appl Nanosci 10:3057–3074. https://doi.org/10.1007/s13204-020-01382-2
40. Ramesh AV, Pavankumar Y, Lavakusa B, Basavaiah K (2017) A facile green synthesis of ZnO nanorods using leaf extract of *Ficus hispida* L. Int J Eng Appl Sci Technol 2(4):256–260. https://www.ijeast.com/papers/256-260,Tesma204,IJEAST.pdf
41. Rahimi Kalateh Shah Mohammad G, Homayouni Tabrizi M, Ardalan T et al (2019) Green synthesis of zinc oxide nanoparticles and evaluation of anti-angiogenesis, anti-inflammatory and cytotoxicity properties. J Biosci 44:30. https://doi.org/10.1007/s12038-019-9845-y.
42. Sangeetha G, Rajeshwari S, Venckatesh R (2011) Green synthesis of zinc oxide nanoparticles by *Aloe barbadensis* miller leaf extract: structure and optical properties. Mater Res Bull 46(12):2560–2566. https://doi.org/10.1016/j.materresbull.2011.07.046
43. M Awwad A, Albiss B, L Ahmad A (2014) Green synthesis, characterization and optical properties of zinc oxide nanosheets using *Olea europea* leaf extract. Adv Mater Lett 5(9):520–524. https://doi.org/10.5185/amlett.2014.5575
44. El-Khawaga AM, Elsayed MA, Gobara M et al (2023) Green synthesized ZnO nanoparticles by *Saccharomyces cerevisiae* and their antibacterial activity and photocatalytic degradation. Biomass Conv Bioref. https://doi.org/10.1007/s13399-023-04827-0
45. Barzinjy AA, Azeez HH (2020) Green synthesis and characterization of zinc oxide nanoparticles using *Eucalyptus globulus* Labill. leaf extract and zinc nitrate hexahydrate salt. SN Appl Sci 2:991. https://doi.org/10.1007/s42452-020-2813-1
46. Khan AU, Malik N, Singh B et al (2023) Biosynthesis, and characterization of zinc oxide nanoparticles (ZnONPs) obtained from

the extract of waste of strawberry. J Umm Al-Qura Univ Appll Sci 9:268–275. https://doi.org/10.1007/s43994-023-00038-5
47. Rajakumar G, Thiruvengadam M, Mydhili G et al (2018) Green approach for synthesis of zinc oxide nanoparticles from *Andrographis paniculata* leaf extract and evaluation of their antioxidant, anti-diabetic, and anti-inflammatory activities. Bioprocess Biosyst Eng 41:21–30. https://doi.org/10.1007/s00449-017-1840-9
48. Raghavendra VB, Shankar S, Govindappa M et al (2022) Green synthesis of zinc oxide nanoparticles (ZnO NPs) for effective degradation of dye, polyethylene and antibacterial performance in waste water treatment. J Inorg Organomet Polym 32:614–630. https://doi.org/10.1007/s10904-021-02142-7
49. Ambika S, Sundrarajan M (2015) Antibacterial behaviour of *Vitex negundo* extract assisted ZnO nanoparticles against pathogenic bacteria. J Photochem Photobiol, B 146:52–57. https://doi.org/10.1016/j.jphotobiol.2015.02.020
50. Rajendrachari S, Taslimi P, Karaoglanli AC, Uzun O, Alp E, Jayaprakash GK (2021) Photocatalytic degradation of Rhodamine B (RhB) dye in waste water and enzymatic inhibition study using cauliflower shaped ZnO nanoparticles synthesized by a novel one-pot green synthesis method. Arab J Chem 14(6):103180. https://doi.org/10.1016/j.arabjc.2021.103180
51. Alshamsi HA, Jaffer AA (2022, November) New *Hibiscus sabdariffa* L. petals extract based green synthesis of zinc oxide nanoparticles for photocatalytic degradation of Rhodamine B dye under solar light. In AIP Conference Proceedings (Vol. 2394, No. 1). AIP Publishing. https://doi.org/10.1063/5.0121228
52. Hazim K, Hamza Z, Mohamed L (2022) Eco-friendly synthesis, antibacterial activity, and photocatalytic performance of ZnO nanoparticles synthesized via leaves extract of Paraserianthes lophantha. Pak J Med Health Sci 16(03):581–581. https://doi.org/10.53350/pjmhs22163581
53. Surendra TV, Roopan SM, Al-Dhabi NA, Arasu MV, Sarkar G, Suthindhiran K (2016) Vegetable peel waste for the production of ZnO nanoparticles and its toxicological efficiency, antifungal, hemolytic, and antibacterial activities. Nanoscale Res Lett 11:1–10. https://doi.org/10.1186/s11671-016-1750-9
54. Karthik P, Ravichandran S, Mukkannan A, Rajesh J (2022) Plant-mediated biosynthesis of zinc oxide nanoparticles from *Delonix elata*: a promising photocatalyst for crystal violet degradation. Inorg Chem Commun 146:110122. https://doi.org/10.1016/j.inoche.2022.110122
55. Khalil AT, Hameed S, Afridi S, Mohamed HEA, Shinwari ZK (2021) *Sageretia thea* mediated biosynthesis of metal oxide nanoparticles for catalytic degradation of crystal violet dye. Mater Today: Proc 36:397–400. https://doi.org/10.1016/j.matpr.2020.04.687
56. Badma Priya D, Thirumalai D, Asharani IV (2021) Influence of synthetic parameters on the enhanced photocatalytic properties of ZnO nanoparticles for the degradation of organic dyes: a green approach. J Mater Sci: Mater Electron 32:9956–9971. https://doi.org/10.1007/s10854-021-05654-7
57. Jones N, Ray B, Ranjit KT, Manna AC (2008) Antibacterial activity of ZnO nanoparticle suspensions on a broad spectrum of microorganisms. FEMS Microbiol Lett 279(1):71–76.39. https://doi.org/10.1111/j.1574-6968.2007.01012.x
58. da Silva BL, Caetano BL, Chiari-Andreo BG (2019) Linhari Rodrigues Pietro RC, Chiavacci LA, Increased antibacterial activity of ZnO nanoparticles: influence of size and surface modification. Colloids Surf, B. https://doi.org/10.1016/j.colsurfb.2019.02.013
59. Arvanag FM, Bayrami A, Habibi-Yangjeh A, Pouran SR (2019) A comprehensive study on antidiabetic and antibacterial activities of ZnO nanoparticles biosynthesized using *Silybum marianum L* seed extract. Mater Sci Eng, C 97:397–405. https://doi.org/10.1016/j.msec.2018.12.058